Environ Earth Sci (2013) 69:1549–1558
DOI 10.1007/s12665-012-1989-0

ORIGINAL ARTICLE

# Multiscale remote-sensing retrieval in the evapotranspiration of *Haloxylon ammodendron* in the Gurbantunggut desert, China

**Xiaoming Cao · Juanle Wang · Xi Chen · Zhiqiang Gao · Fei Yang · Jiankang Shi**

Received: 7 February 2012 / Accepted: 11 September 2012 / Published online: 21 September 2012


**Abstract** Transpiration, an essential component of surface evapotranspiration, is particularly important in the research of surface evapotranspiration in arid areas. The paper explores the spectral information of the arid vegetal evapotranspiration from a semi-empirical perspective by the measured data and the up-scaling method. The paper inverted the transpiration of *Haloxylon ammodendron* at the canopy, pixel and regional scales in the southern edge of the Gurbantunggut desert in Xinjiang, China. The results are as follows: at the canopy scale, the optimal exponential model of the sap flow rate based on the hyperspectrum is $y = 0.0015e^{3.8922x}$, $R^2 = 0.806$. At the pixel scale, there was a good linear relationship between the sap flow and the SR index, with a relationship of $y = -1197.38x^3 + 1048.43x^2 - 305.47x + 455.15$, $R^2 = 0.845$. At the regional scale, based on the optimal exponential model and the EO-1 Hyperion remote-sensing data, the transpiration of the study area was inverted. Comparing the results of the SEBAL and SEBS models, the errors of the simulation results were 7.78 and 8.80 %. The paper made full use of the knowledge flow at different scales, bridging the scale difference in canopy and remote-sensing images to avoid the information bottleneck in the up-scaling. However, there are many constraints in the data acquirement, the efficiency of the models, the endmembers determination, the temporal–spatial up-scaling, and the accuracy assessment, which would be improved in future studies.

**Keywords** Evapotranspiration · Scale · Remote sensing · *Haloxylon ammodendron* · The arid areas

X. Cao · J. Wang (✉) · F. Yang
State Key Laboratory of Resources and Environmental Information Systems, Institute of Geographical Sciences and Natural Resources Research, Chinese Academy of Sciences, Beijing 100101, China
e-mail: wangjl@igsnrr.ac.cn

X. Cao
e-mail: caoxm1027@gmail.com

F. Yang
e-mail: yangfei@lreis.ac.cn

X. Chen
Xinjiang Institute of Ecology and Geography, Chinese Academy of Science, Urumqi 830011, China
e-mail: chenxi@ms.xjb.ac.cn

Z. Gao
Yantai Institute of Coastal Zone Research, Chinese Academy of Science, Yantai 264003, China
e-mail: gaozq@igsnrr.ac.cn

J. Shi
Hainan Research Academy of Environmental Sciences, Haikou, China
e-mail: stanking16888@163.com

## Introduction

Evapotranspiration (ET) is the final stage of water consumption in the inland water cycle of arid land. Transpiration plays a critical role in the configuration of water resources in arid land and the maintenance of the energy balance in the ecological system (Bodner et al. 2007).

Researchers studied surface ET at different scales with the general measurement method and estimation method. At the plant scale, various measurement methods, including weighing lysimeters, ventilated chambers, radioisotopes, stable isotopes and heat balance/heat dissipation methods have been proven to be valuable tools for conducting basic and applied research (Wullschleger et al. 1998). Sap flow instruments, the effective techniques to

measure plant transpiration (Hatton et al. 1995; Vertessy et al. 1997), have been used to study the transpiration of *Haloxylon ammodendron* and *Tamarix ramosissima* in Taklimakan desert (Xu 2006; Xu et al. 2008). At stand scale, the thermal pulse method has been effectively used to measure the stem sap flow of sub-deciduous (Wullschleger et al. 2001; Zhang and Gong 2004; Zhang et al. 2005). Cleverly et al. (2002) estimated the seasonal actual ET from *Tamarix ramosissima* stands using three-dimensional eddy covariance. Moore et al. (2008) estimated nocturnal transpiration in riparian *Tamarix* thickets authenticated by sap flux, eddy covariance and leaf gas exchange measurements. Moreover, the Penman–Monteith equation and a modified Jarvis–Stewart model are effective to estimate stand and canopy-scale transpiration (Whitley et al. 2009). At the patch scale, Stannard (1993) suggested that it was effective to estimate the ET of wildland vegetation in semi-arid rangeland using the Penman–Monteith equation and the Shuttleworth–Wallace and modified Priestley–Taylor ET models. Comparison of the measured transpiration of a mixed spruce–aspen–birch forest did not show any significant differences between the estimated value of the more sophisticated mixed forest multi-layer SVAT (soil–vegetation–atmosphere-transfer) model (MF-SVAT) and the simple multi-layer (ML-SVAT) under sufficient soil moisture conditions; however, ML-SVAT overestimated it under limited soil moisture conditions (Oltchev et al. 2002). In semi-arid land, estimating cover crop ET using the Food and Agriculture Organization (FAO) dual crop coefficient method with water stress compensation was found to be effective (Bodner et al. 2007).

In addition, remote sensing is considered an effective way to study the problem of spatial scale, and researchers have proposed the estimated ET model based on the surface energy balance equation. In 1973, based on the energy balance and the principles of crop resistance, Brown proposed the crop resistance-evapotranspiration model, which provided a theoretical basis for the application of thermal infrared remote sensing in ET inversion (Brown and Rosenberg 1973). Subsequently, Bastiaanssen published a series of papers on ET estimation based on the SEBAL (Bastiaanssen et al. 1998a, b; Bastiaanssen 2000) model using Landsat TM remote-sensing images, which have been widely used in different studies (Allen et al. 2005; Morse et al. 2000; Bastiaanssen and Bandara 2001). Hyperspectral remote-sensing data provide ample information in the physiology ecology characteristics of vegetation (Thomas 1977). More researches have focused on the deeper reflectance response of vegetation water to invert vegetation water use, and much progress has been made (Ceccato et al. 2001; Penuelas et al. 1993). However, ET estimated by hyperspectral remote-sensing data has not been reported. Moreover, due to the variation of scales, studies combining measurement methods at the canopy scale and remote-sensing methods at the regional scale are still relatively weak.

*Haloxylon ammodendron* is a dominant native desert shrub in central Asia. It is widely distributed in the Gurbantunggut desert on the northern slope of Tianshan Mountain. *Haloxylon ammodendron* has adapted well to high temperature and drought due to its degenerated scale leaves, which act as an assimilation organ (Xu et al. 2007) (Fig. 1a). Studies on *Haloxylon ammodendron* have focused on factors such as ecological environment, distribution, physical characteristics and the water balance (Wang and Ma 2003). Researchers have widely studied the ET of *Haloxylon ammodendron* at the canopy and stand scales (Zhang et al. 2003; 2005; Zhang and Gong 2004; Xu 2006; Xu et al. 2008). However, due to the complexity inherent in the process of ET in arid lands, and the difficulties in the up-scaling in different scales, there are no studies focusing on ET simulation of the dominant native desert shrub based on the hyperspectral remote-sensing data.

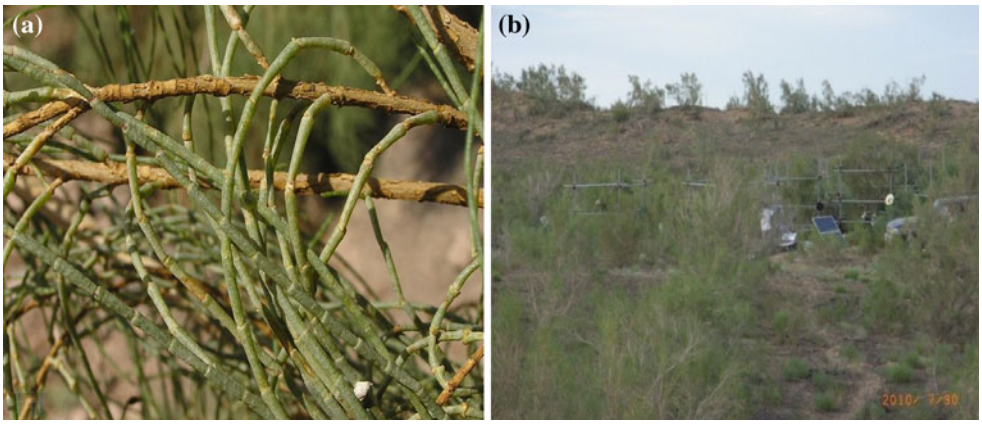


**Fig. 1** The assimilation organ of *Haloxylon ammodendron* (**a**) and the natural landscape of the quadrat (**b**)

Base on the measurement data and the remote sensing method, the paper investigates the spectral responses of the transpiration of *Haloxylon ammodendron* in the Gurbantunggut desert at the canopy scale, pixel scale and regional scale. Through scale deduction, the ET of *Haloxylon ammodendron* on the southern edge of the Gurbantunggut desert is inverted using an EO-1 Hyperion remote-sensing image.

## Methods

### The study area

The study area is located at the southern edge of the Gurbantunggut desert on the northern slope of the Tianshan Mountains, where a large area is occupied by native saline desert vegetation (Cao et al. 2011). The climate is temperate zone continental desert, where it is hot and dry in summer and cold in winter. The average annual temperature is 6.6 °C, the average precipitation is 160 mm, and the average annual ET is 2,000 mm (Xu et al. 2007). Precipitation and soil water are the main water sources for the vegetation. Typical desert subshrubs such as *Haloxylon ammodendron* are distributed here, and it is an important area for ecological processes and preservation in arid central Asia (Fig. 2).

### Data

To acquire the measured data, the study set up a quadrat (30 × 30 m) in the desert (44°25′56.5″N, 87°54′13.0″E, altitude 468 m), 10 km from the southern edge of the desert (Figs. 1b, 2). There are a total of 36 *Haloxylon ammodendron* in the quadrat of which 10 adults were selected randomly for monitoring. The experiments were carried out from July 2009 to November 2010. The data included three parts:

#### *The stem sap flow rate*

The stem sap flow rate of *Haloxylon ammodendron* was measured by Sakuratani (1984) sap flow gauges, which were based on the heat balance method (Sakuratani 1981). A DT Logger80 was used to record and store the average data every 10 min. The diameters of all the branches were measured using a micrometer. The physical parameters of the each *Haloxylon ammodendron* in the quadrat (e.g., the height, the crown diameters, the stem base diameters) were also measured by a tape.

#### *The remote-sensing data*

The remote-sensing data included the measured reflectance of the canopy and the soil, an EO-1 Hyperion remote-sensing

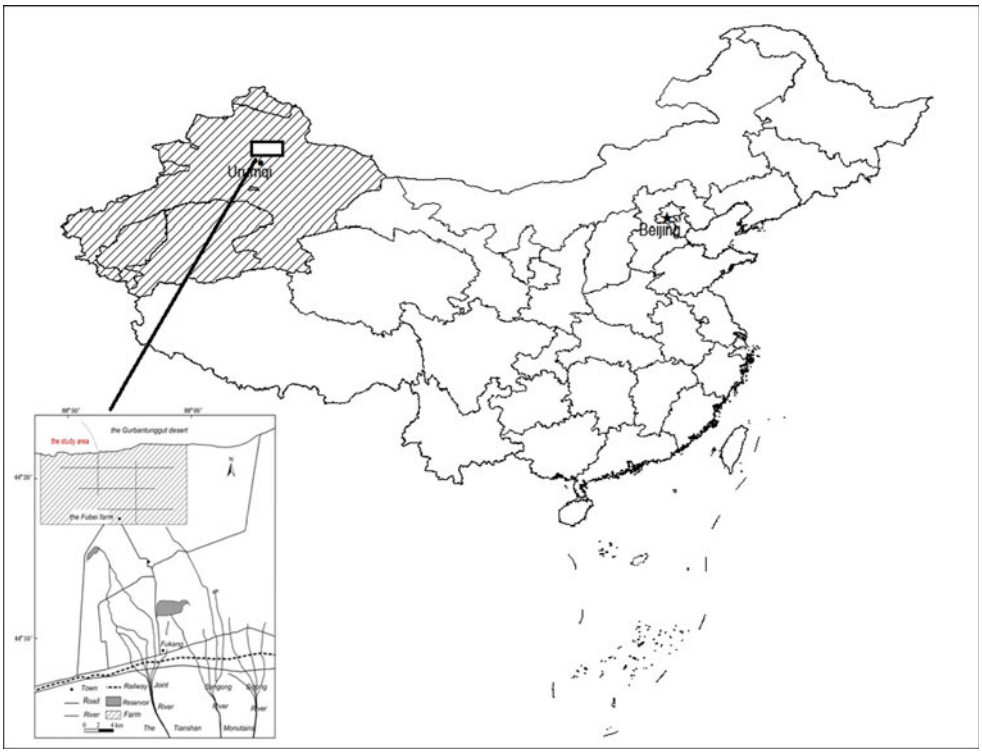


**Fig. 2** The study area

image. The measured reflectance was collected by an ASD FieldSpec Pro spectrometer with a spectral range of 350–2,500 nm and a spectral interval of 1 nm. The measured reflectance data were collected during local time from 10:00 to 14:00, with sunshine and cloud cover less than 5 %, on Jul 30 (T1), Aug 26 (T2) and Sept 17 (T3), 2009, and May 29 (T4), Jul 1 (T5), Aug 10 (T6) and Sept 17 (T7), 2010 (all times reported in the paper are local time). An EO-1 Hyperion remote-sensing image was acquired at 11:00 on May 12, 2009, from USGS with the L1R format and a track number of 142/29.

### *The meteorological data*

The meteorological data, including average temperature, maximum temperature, minimum temperature, relative humidity, dew point, wind speed, wind direction, barometric pressure, rainfall, solar radiation and radiation energy, were collected at an interval of 0.5 h by a portable automatic weather station (Vantage Pro2TM).

## Data processing

### *Calculation of vegetation transpiration*

The vegetation transpiration was calculated using the cross-sectional area method (Vertessy et al. 1995, 1997):

$$Q = \frac{f}{s} \times S_A \times H \tag{1}$$

where $s$ ($cm^2$) is the cross-sectional area of the branch installed a sap flow gauge; $S_A$ ($cm^2$) is the total cross-sectional area of one plant; all the cross-sectional area was calculated from the diameters of the branches; $f$ (g/h) is the stem sap flow rate of the branch installed a sap flow gauge; $H$ (h) is the period of collecting the stem sap flow rate; $Q$ (g) is the single-plant water consumption during the period of $H$.

### *EO-1 Hyperion remote-sensing image data processing*

All processes, including effective band selection, band line repair, smile correction (Goodenough et al. 2003), atmospheric correction and geometric correction, can be found in Zhang and Micha (2007). The endmembers were extracted from the image using the purity pixel index method (PPI) (Rogge et al. 2007; Plaza et al. 2004). Due to the single vegetation cover, the problem of mixed pixels was not significant. The vegetation endmembers were extracted from the croplands because of the scarcity of the vegetation in the desert. The reflectance of the endmembers was confirmed based on the spectral library in the ENVI software and interpretation of the image. Finally, the pixels were unmixed based on the constraints of minimum energy.

## Introduction of the algorithm

### *Calculation and determination of the best spectral index*

Regression analysis is the most widely used empirical method to study the relationship between two variables (Cohen et al. 2003). In general, one variable is difficult or costly to obtain (e.g., sap flow rate), while the other one is relatively easily to obtain (e.g., the measured reflectance of vegetation). In the paper, the regression analysis was used to explore the sensitive bands or bands combination to sap flow rate from 350 to 2,500 nm. Four types of spectral index, ranging from the very simple ($R$) to more sophisticated (ND type) specifically designed to quantify the sap flow rate, were applied in the paper (Table 1). Firstly, the best wavelength domains for a given type of index by screening all combinations using correlation analysis based on measurements were determined; and then the best one was identified from the four types of indices. Each index was calculated by a step size of 5 nm.

A 2-D $R^2$ graph has been presented, a two-dimensional contour plot of the coefficient of determination ($R^2$) with the two wavelengths on the $x$ and $y$ axes. The map provided an overview of the statistical significance of SR for all combination of two wavelengths. It allows efficient extraction of significant peak-wavelengths as well as the extent of the effective regions for assessment of each target variable.

A linear regression was then fitted between the indices and the sap flow rate. The authors have also tried fitting with higher order polynomials while no significant improvement has been obtained. The coefficient of determination ($R^2$) is applied as the criterion to identify the best index.

$$R^2 = 1 - \sum_{i=1}^{n} (y_i' - \bar{y})^2 - \sum_{i=1}^{n} (y_i - \bar{y})^2 \tag{2}$$

$$\mathrm{RMSE} = \sqrt{\frac{\sum_{i=1}^{n} (y_i' - \bar{y})^2}{n}} \tag{3}$$

**Table 1** The spectral indices used in the paper

| The spectral indices | The formula |
|---|---|
| Reflectance ($R$) | $\rho\lambda_1$ |
| Difference ($D$) | $\rho\lambda_1 - \rho\lambda_2$ |
| Simple ratio (SR) | $\rho\lambda_1/\rho\lambda_2$ |
| Normalized difference (ND) | $(\rho\lambda_1 - \rho\lambda_2)/(\rho\lambda_1 + \rho\lambda_2)$ |

$\lambda_1$, $\lambda_2$ is the wavelength, and $\rho\lambda_1$, $\rho\lambda_2$ is the corresponding reflectance

where $R^2$ is the coefficient of determination, $y'$ is the estimated value, $y$ is the independent reference measurement, and root-mean-square error (RMSE) is the absolute error in estimation. The group of $\lambda_1$, $\lambda_2$ with the maximum $R^2$ formed the optimum spectral index. All the work was performed in MATLAB.

*Linear mixed model*

The linear mixed model, the most common method to unmix endmembers, is defined as follows: the reflectance of a spectral band is the linear combination of the reflectance of every endmember (Zhao 2003). The formula is as follows:

$$R_{i\lambda} = \sum_{K=1}^{n} f_{ki} C_{k\lambda} + \varepsilon_{i\lambda} \quad (4)$$

$$\sum_{k=1}^{n} f_{ki} = 1 \quad (\mathrm{k} = 1,\ 2,\ 3\ldots n) \quad (5)$$

where $R_{i\lambda}$ is the spectral reflectance of the pixel $i$ in band $\lambda$ (known); $f_{ki}$ is the weight of the endmember $k$ for the pixel $i$ (unknown); $C_{k\lambda}$ is the spectral reflectance of the endmember $k$ in band $\lambda$; $\varepsilon_{i\lambda}$ is the residual error (the unmodeled spectrum); $n$ is the number of the endmembers; $m$ is the used bands, $n \leq (m + 1)$, so that the least square method could be used.

The pixel reflectance is decided by the vegetation and the soil. The reflectance of the two endmembers is calculated by the measured reflectance of the vegetation and the soil. The vegetation fractional cover ($F_c$) is calculated by the measured physical parameters of *Haloxylon ammodendron*.

*The cosine function*

Fredrik and Anders (2002) showed that the daily transpiration is equal to the daily sap flow. At the daily scale, therefore, sap flow could be used to measure transpiration and characterize the transpiration and water consumption of one plant. On sunny days, the microclimate exhibits regular changes over a 24-h period (Xu et al. 2008). Jackson et al. (1983) put forward that daily ET could be calculated by the sine function based on latitude and longitude values, time and instantaneous ET. Based on the sine or cosine changes of the daily solar radiation flux density, Xie (1991) put forward that there was a sine or cosine relationship between daily and instantaneous ET values.

$$F'_{(t)} = F_0 + F_a \cos(0.5\pi \times (t - t_m/P_d) \quad (6)$$

where $F'_{(t)}$ is the simulated sap flow rate (mm/h); $F_0$ is the daily average sap flow rate (mm/h) (known); $F_a$ is the maximum daily sap flow rate (known); $t_m$ is the time when $F_a$ appears, which could be collected from the meteorological data and the stem sap flow rate; $P_d$ is the sunshine hours (h), which was measured by the portable automatic weather station (Vantage Pro2TM).

This paper introduces the error factor $\sigma$ to improve the simulation accuracy. $\sigma$ is calculated by the following formula:

$$\sigma = \frac{F_{m(t)} - F'_{(t)}}{F_{m(t)}} \quad (7)$$

where $F_{m(t)}$ is the sap flow rate at time $t$. The simulated sap flow rate by the modified cosine function is as follows:

$$F_{(t)} = (1 + \sigma) \times F'_{(t)}. \quad (8)$$

## The results

### The spectral response of the sap flow rate at the canopy scale

The spectral response of the sap flow rate was studied (30 points) based on the measured canopy reflectance and the corresponding average sap flow rate. Table 2 presents the highest $R^2$, wavelength(s), RMSE and P for each spectral index.

A statistically significant correlation ($R^2 > 0.43$, $P < 0.0001$) to the sap flow rate could be shown for all indices derived from spectra taken from the canopy (Table 2). The correlation coefficients between the measured sap flow rate and spectral indices varied among indices ($R^2 = 0.43$–$0.62$). SR showed the highest correlation coefficient ($R^2 = 0.62$) to all measured sap flow rate,

**Table 2** The sensitive bands of every spectral index

| The spectral index | $\lambda_1$ (nm) | $\lambda_2$ (nm) | $a$ | $b$ | $R^2$ | RMSE (kg/h) | $P$ |
|---|---|---|---|---|---|---|---|
| $R$ | 1,970 | – | 8.24 | −0.14 | 0.43 | 1.358 | <0.0001 |
| $D$ | 2,070 | 2,310 | 7.81 | −0.93 | 0.48 | 1.395 | <0.0001 |
| SR | 1,580 | 1,600 | 0.76 | 3.65 | 0.62 | 1.124 | <0.0001 |
| ND | 1,580 | 1,600 | 4.37 | 16.61 | 0.61 | 1.167 | <0.0001 |

followed by ND ($R^2 = 0.61$). SR and ND had a similar $R^2$; however, the RMSE of SR (RMSE = 1.124 kg/h) was much smaller than that of ND (RMSE = 1.167 kg/h). Substantially lower correlation coefficients could be observed for $D$ ($R^2 = 0.48$, RMSE = 1.358 kg/h) and $R$ ($R^2 = 0.43$, RMSE = 1.395 kg/h).

Because of its simplicity, significant correlation coefficient and lowest RMSE, the SR index is used as the sensitivity index for the sap flow rate estimation. Figure 3 provides an overview of the statistical significance of SR for all combinations of two wavelengths. There are several narrow parks (reddish) and broad regions (yellowish). The first region, 750–1,310 versus 1,380–1,500 nm, has the highest $R^2$ values. The second region of high $R^2$ values is approximately 1,540–1,600 versus 1,550–1,700 nm. The third region of high $R^2$ values is approximately 350–750 versus 700–1,150 nm. However, the 1,380–1,500 nm region is within the atmospheric window, it cannot be used with remote-sensing images. The second region (1,540–1,600 versus 1,550–1,700 nm) was selected as the SR index. Figure 3 reveals that the SR spectral index calculated by the reflectance at 1,580 and 1,600 nm has the highest $R^2$, which was used with remote-sensing images.

Based on the least square method (Das and Basudhar 2006), the relationship between the measured canopy sap flow rate and $SR_{(1,580,1,600)}$ was fitted by several fitting types, including simple linear regression, quadratic polynomial, cubic polynomial, logarithmic equation, index equation and power function (Table 3). Table 3 reveals a good relationship between them, with the maximum $R^2$ of 0.806 and the minimum $R^2$ of 0.650. There was the most significant relationship between sap flow rate and SR by index function ($R^2 = 0.806$, $P < 0.001$), with the equation of $y = 0.0015e^{3.8922x}$.

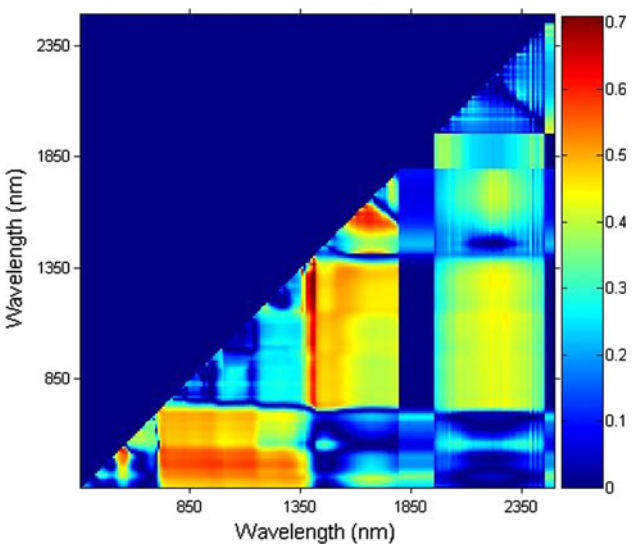


**Fig. 3** Matrix representing the $R^2$ of sap flow rate

**Table 3** The fitting models between the measured canopy sap flow and $SR_{(1,580,1,600)}$

| Fitting type | The models | $R^2$ | $P$ |
|---|---|---|---|
| Simple linear | $y = 3.405x - 4.423$ | 0.722 | 0.001 |
| Quadratic polynomial | $y = 4.736x^2 - 11.53x + 7.208$ | 0.742 | <0.001 |
| Cubic polynomial | $y = -12.365x^3 + 63.7x^2 - 104.41x + 55.51$ | 0.754 | <0.001 |
| Logarithmic equation | $y = 5.214\ln(x) - 1.393$ | 0.650 | 0.001 |
| Index equation | $y = 0.0015e^{3.8922x}$ | 0.806 | <0.001 |
| Power function | $y = 0.047x^{6.0528}$ | 0.791 | <0.001 |

## Spectral response of the sap flow at the pixel scale

Based on the measured reflectance of each endmember and the measured $F_c$, the reflectance of the quadrat at each sampling time was simulated by the mixed liner model (Fig. 4a), which was used as the EO-1 Hyperion equivalent reflectance.

Considering the good fit of the SR index at the canopy scale, the paper used the least square method to fit the relationship between SR and the measured average sap flow rate of the quadrat at the pixel scale (Table 4). Table 4 reveals a good relationship between them, with the maximum $R^2$ of 0.845 and the minimum $R^2$ of 0.485. There was the most significant relationship between sap flow rate and SR by index function ($R^2 = 0.845$, $P < 0.001$), with the equation of $y = -1197.38x^3 + 1048.43x^2 - 305.47x + 455.15$ (Fig. 4b).

## The inversion of ET at the regional scale

### *The inversion results*

The average sap flow rate was estimated based on the best index model, $y = -1197.38 \times SR^3_{(1,580,1,600)} + 1048.43 \times SR^2_{(1,580,1,600)} - 305.47 \times SR_{(1,580,1,600)} + 455.15$ and the EO-1 Hyperion remote-sensing image of May 12, 2009. Figure 5 reveals that the sap flow rate was higher at the edge of the oasis, varying from 0.060 to 0.100 mm/h (orange), values that were obviously higher than in the desert. In some areas covered by winter wheat and agricultural afforestation, the sap flow rate was even higher than 0.100 mm/h (reddish). In the desert, the sap flow rate was relatively lower: in the area with higher vegetation cover (blue), the sap flow rate varied from 0.030 mm/h to 0.060 mm/h, whereas in areas with low vegetation cover (iridescent and yellowish), the sap flow rate was lower than

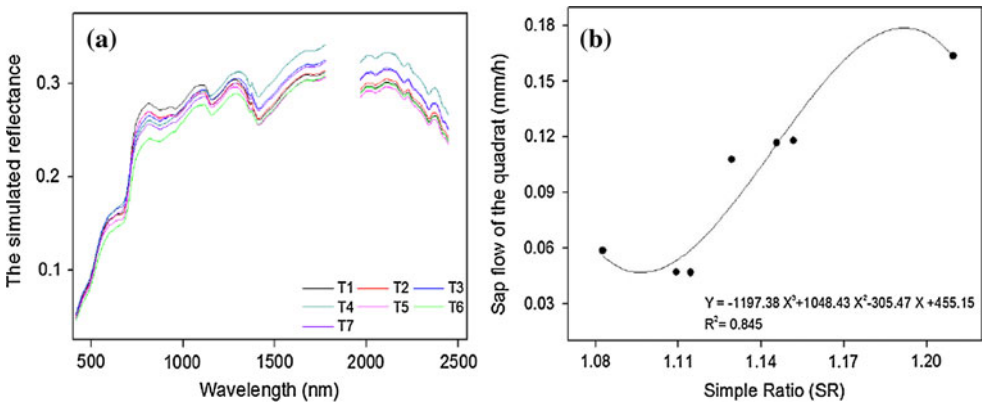


**Fig. 4** The simulated reflectance of the quadrat (**a**) and the relation between the average sap flow and SR (**b**)

**Table 4** The fitting models between the average sap flow and SR in pixel scale

| Fitting type | The models | $R^2$ | $P$ |
|---|---|---|---|
| Simple linear | $y = 1.049x - 1.101$ | 0.661 | 0.001 |
| Quadratic polynomial | $y = -2.614x^2 + 7.052x - 4.542$ | 0.669 | <0.001 |
| Cubic polynomial | $y = -1197.38x^3 + 1048.43x^2 - 305.47x + 455.15$ | 0.845 | <0.001 |
| Logarithmic equation | $y = 1.205\ln(x) - 0.0617$ | 0.664 | 0.001 |
| Index equation | $y = 0.012 \times 14.81$ | 0.486 | <0.001 |
| Power function | $y = 3 \times 10^{-8} \times e^{12.89x}$ | 0.485 | <0.001 |

0.030 mm/h. Based on the latitude and longitude, the sap flow rate of the quadrat extracted in ArcGIS was 0.0387 mm/h.

*Time up-scaling of ET*

The daily ET in the study area on May 12, 2009, was simulated by the modified cosine function from the instantaneous ET (Fig. 6). Due to the lack of measured sap flow data in May 2009, the period of May 10–20, 2010, was taken as the study period to determine $\sigma$, which was found to be 0.2537. Figure 6 shows the simulated daily sap flow using the modified cosine function.

Figure 6 shows that the modified cosine function simulated the daily stem sap flow more accurately. However, $\sigma$ changed with the changes of vegetation growth and environment; therefore, it was not constant over a long period. In this paper, $\sigma$ was only used for a short period during sunny days when there was little change in temperature, no rainfall, and relatively stable soil moisture content. The daily sap flow on May 12, 2009, simulated with $\sigma$ was determined as 0.6912. Due to the simplicity of the vegetation cover, the daily soil evaporation was treated as a constant, which was 0.6 mm (Zhai et al. 2007). Therefore, the daily ET of the quadrat on May 12, 2009, was calculated as 0.6460 mm.

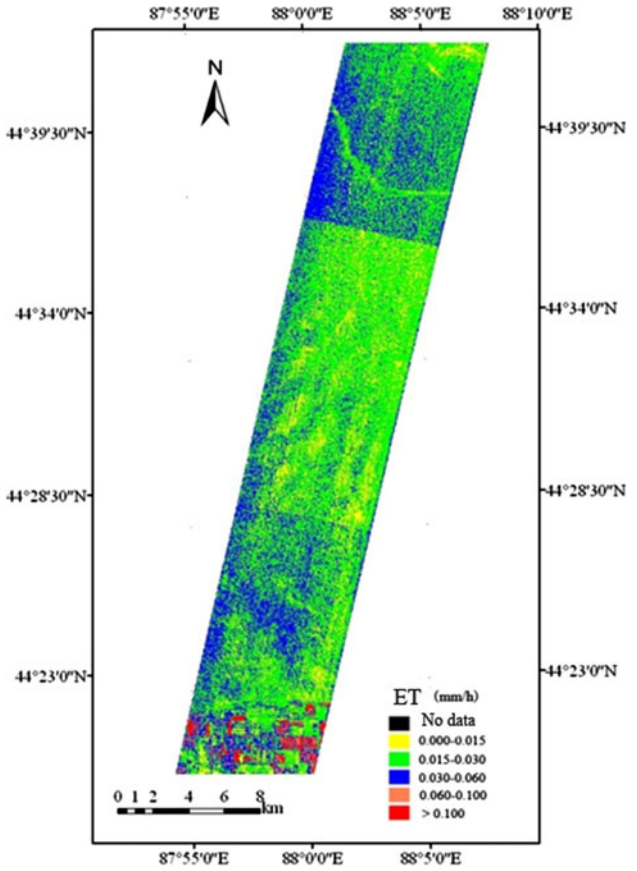


**Fig. 5** The evapotranspiration of *Haloxylon ammodendron* in the study area

*Accuracy assessment*

Due to lack of measured ET data on May 12, 2009, the ET on May 24, 2007, simulated by the SEBS (Su 2000, 2002) model and the SEBAL models (Li 2010), was used to assess the results. The simulated ET by the SEBS and SEBAL models of the quadrat was extracted by ArcGIS as 0.5958 and 0.5892 mm, respectively (Table 5). Table 5 shows that the difference of the SEBS and SEBAL models

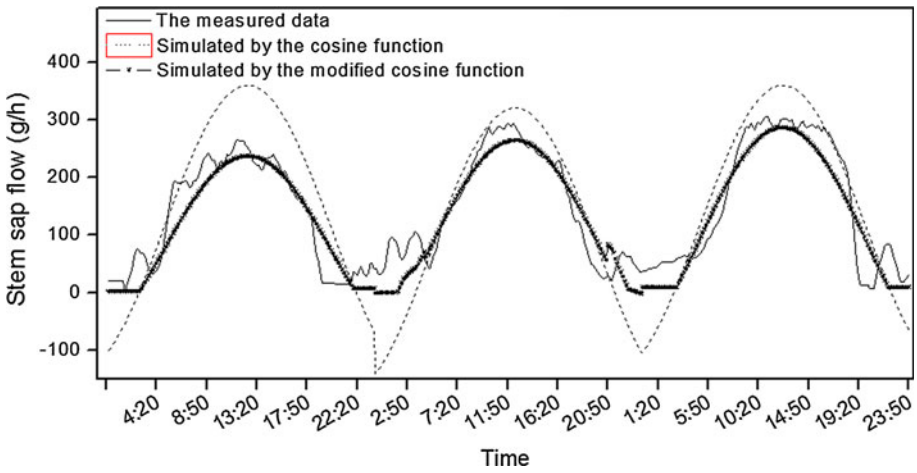


**Fig. 6** The comparison of the simulated and measured stem sap flow rate

**Table 5** Accuracy assessment of the optimum index, SEBS and SEBAL models

| The optimum model (mm) | SEBS model (mm) | SEBAL model (mm) | Comparison with SEBS | | Comparison with SEBAL | |
|---|---|---|---|---|---|---|
| | | | $\lvert\Delta_{\text{optimum-SEBS}}\rvert$ | Error | $\lvert\Delta_{\text{optimum-SEBAL}}\rvert$ | Error |
| 0.6460 | 0.5958 | 0.5892 | 0.0502 | 7.78 % | 0.0568 | 8.80 % |

was 7.78 and 8.80 %, respectively. Therefore, based on the optimum index, $y = -1197.38 \times SR^3_{(1,580,1,600)} + 1048.43 \times SR^2_{(1,580,1,600)} - 305.47 \times SR_{(1,580,1,600)} + 455.15$, and the EO-1 Hyperion remote-sensing image, the sap flow rate could be estimated accurately. Consequently, the daily ET could be calculated by the modified cosine function.

## Discussion and conclusion

### ET inversion by hyperspectral remote-sensing data

The biophysical and biochemical parameters largely affect the water consumption of vegetation (Asner 1998). The acquisition of reflectance is helpful for studying the spectral characteristics and physical mechanisms of ET (Green et al. 1996). The results of this paper reveal that the bands most sensitive to reflectance for the sap flow are the visible and near infrared bands, such as 350–750 versus 700–1,150 nm, 750–1,310 nm vs. 1,380–1,500 nm, and 1,540–1,600 nm vs. 1,550–1,700 nm. Based on these results, a hyperspectral inversion model, $y = 0.0015e^{3.8922x}$, was established at the canopy scale. This approach focuses on excavating the spectral information to explore the vegetal ET for the first time, despite plenty of studies concerning the spectral information of the water content (Ceccato et al. 2001), photosynthesis (Sellers 1987; Zhao et al. 2005), etc. Moreover, it is more suitable for arid desert areas with obvious constructive species, because of the lower vegetation cover and the single community. Due to the differences of the biophysical and biochemical parameters of the different vegetation types, the inversion model established in the paper can only be used for specific vegetation types. More fieldwork is needed to obtain spectral information and other parameters, factors that caused difficulty in the study.

### The scale effect in the inversion of ET

Considering the differences in the different scales, this paper simulated ET at the spatial and time scales. At the canopy scale, the optimum index model was established by the iteration method instead of the typical measurement (Wullschleger et al. 2001; Cleverly et al. 2002; Xu et al. 2008) and estimation (Penuelas et al. 1993; Bodner et al. 2007). The hyperspectral response characteristics of the sap flow rate were first explored from the semi-empirical perspective. It was then proved that the sap flow rate can be estimated by the corresponding measured canopy reflectance. At the pixel scale, the paper successfully estimated the reflectance with the linear mixed model, and the sap flow rate with the measured $F_c$. The sap flow inversion model at the pixel scale, $y = -1197.38 \times SR^3_{(1,580,1,600)} + 1048.43 \times SR^2_{(1,580,1,600)} - 305.47 \times SR_{(1,580,1,600)} + 455.15$, was then established. Finally, the regional ET was inverted by hyperspectral remote sensing. The paper studied the ET inversion method from a semi-empirical perspective by the measured data and the up-scaling method instead of the typical surface energy balance equation used at the regional scale. This approach made full use of the knowledge flow at different scales, bridging the scale difference in canopy

and remote-sensing images to avoid the information bottleneck in the up-scaling.

However, there are several deficiencies to be improved in the future studies. Firstly, there are extreme variations in the phytomorph between *Haloxylon ammodendron* and typical broad-leaved forest or coniferous forest (Fig. 1a), which would contribute to the difficulties in estimating leaf area index (LAI) and $F_c$. Due to the limited experimental conditions, the authors used measured physical parameters and estimated porosity to calculate $F_c$ in the paper. However, $F_c$ is a vital parameter in the up-scaling studies for quantitative remote sensing. Thus, high-precision measurement and estimation method would be explored in the future studies. Secondly, *Haloxylon ammodendron* is the dominant native desert shrub in the study area and it is the main contribution to the vegetation cover, so only two endmembers, vegetation (*Haloxylon ammodendron*) and soil were considered in the spatial up-scaling study. However, for other areas covered by more species, it is unsuitable. Thirdly, in the temporal up-scaling study, the modified cosine function, with $\sigma$ determined by the meteorological data, simulated the daily sap flow more accurately. The use of $\sigma$ was greatly limited because of the changing meteorological factors. Fourthly, due to the lack of measured ET at the time of satellite transit, the paper used the results of another researcher to assess the accuracy, which should be improved in future studies.

**Acknowledgments** The authors are grateful for the support by Public Welfare Special Program, Ministry of Environmental Protection of the People's Republic of China (Grant No. 201109075); the Research Project of Public Service Sectors from the Ministry of Environment Protection in China (Grant No. 201209030-3): land use spatial and temporal changes and its environmental effects in China; the basic work items by the Ministry of Science the norms for the comprehensive scientific investigation of the grid-based resources and environment of the People's Republic of China (Grant No. 2011FY110400); National Natural Science Foundation of China (41171334 and 41071278). The authors are also grateful for the help in the field work of Professor Quan Wang from Shizuoka University in Japan, Dr. Shanshan Wang from Xinjiang Institute of Ecology and Geography, Chinese Academy of Science.

## References

Allen RG, Tasumi M, Morse A, Trezza R (2005) A Landsat-based energy balance and evapotranspiration model in Western US water rights regulation and planning. Irrigation Drainage Syst 19(3):251–268

Asner GP (1998) Biophysical and biochemical sources of variability in canopy reflectance. Remote Sens Environ 64:234–253

Bastiaanssen WGM (2000) SEBAL-based sensible and latent heat fluxes in the irrigated Gediz Basin Turkey. J Hydrol 229(1–2):87–100

Bastiaanssen WGM, Bandara KMPS (2001) Evaporative depletion assessments for irrigated watersheds in Sri Lanka. Irrig Sci 21(1):1–15

Bastiaanssen WGM, Menenti M, Feddes RA, Holtslag AAM (1998a) A remote sensing surface energy balance algorithm for land (SEBAL). 1 Formulation. J Hydrol 212–213:198–212

Bastiaanssen WGM, Pelgrum H, Wang J (1998b) A remote sensing surface energy balance algorithm for land (SEBAL). 2 Validation. J Hydrol 212–213:213–229

Bodner G, Loiskandl W, Paul HP (2007) Cover crop evapotranspiration under semi-arid conditions using FAO (Food and Agriculture Organization) dual crop coefficient method with water stress compensation. Agric Water Manag 93(3):85–98

Brown KW, Rosenberg NJ (1973) A resistance model to predict evapotranspiration and its application to a sugar beet filed. Agron J 65(3):341–347

Cao XM, Chen X, Bao AM, Wang Q (2011) Response of vegetation to temperature and precipitation in Xinjiang during the period of 1998–2009. J arid land 3(2):94–103

Ceccato P, Flasse S, Tarantola S, Jacquemoud S, Gregoire JM (2001) Detecting vegetation leaf water content using reflectance in the optical domain. Remote Sens Environ 77:22–33

Cleverly JR, Dahm CN, Thibault JR (2002) Seasonal estimates of actual evapo-transpiration from *Tamarix ramosissima* stands using three-dimensional eddy covariance. J Arid Environ 52:181–197

Cohen WB, Maiersperger TK, Gower ST (2003) An improved strategy for regression of biophysical variables and Landsat ETM+data. Remote Sens Environ 84(4):561–571

Das SK, Basudhar PK (2006) Comparison study of parameter estimation techniques for rock failure criterion models. Can Geotech J 43(7):764–771

Fredrik L, Anders L (2002) Transpiration response to soil moisture in pine and spruce trees in Sweden. Agric For Meteorol 112(2): 67–85

Goodenough DG, Dyk A, Niemann KO (2003) Processing Hyperion and ALI for Forest classification. IEEE Trans Geosci Remote Sens 41(6):1321–1331

Green RM, Lucas NS, Curran PJ, Foody GM (1996) Coupling remotely sensed data to an ecosystem simulation model-an example involving a coniferous plantation in upland Wales. Global Ecol Biogeogr Lett 5:192–205

Hatton TJ, Moore SJ, Reece PH (1995) Estimating stand transpiration in a *Eucalyptus populnea* woodland with the heat pulse method: measurement errors and sampling strategies. Tree Physiol 15:219–227

Jackson RD, Hatfield JL, Reginato RJ (1983) Estimation of daily evapotranspiration from one time-of-day measurements. Agric Water Manag 7(1–3):351–362

Li Q (2010) Remote Sensing of Temporal-Spatial Retrieval of the Process of Regional Evapotranspiration in Arid areas. The PHD thesis of the graduate school of Chinese Academy of Sciences

Moore GW, Cleverly JR, Owens MK (2008) Nocturnal transpiration in riparian *Tamarix* thickets authenticated by sap flux, eddy covariance and leaf gas exchange measurements. Tree Physiol 28(4):521–528

Morse A, Tasumi M, Allen RG, Kramber WJ (2000) Application of the SEBAL methodology for estimating consumptive use of Water and streamflow depletion in the Bear river basin of Idaho through Remote Sensing. Final report submitted to the Raytheon Systems Company, Earth Observation System Data and Information system Project, by Idaho Department of Water Resources and University of Idaho

Oltchev A, Cermak J, Nadezhdina N, Nadezhdina N (2002) Transpiration of a mixed forest stand: field measurements and simulation using SVAT models. Boreal Environ 7:1–9

Penuelas J, Filella I, Biel C, Serrano L, Save R (1993) The reflectance at the 950–970 nm region as an indicator of plant water status. Int J Remote Sens 14:1887–1905

Plaza A, Martineaz P, Perez R, Plaza J (2004) A quantitative and comparative analysis of endmember extraction algorithms from hyperspectral data. IEEE Trans Geosci Remote Sens 42(3): 650–663

Rogge DM, Rivard B, Zhang J, Sanchez A (2007) Integration of spatial-spectral information for the improved extraction of endmembers. Remote Sens Environ 110(3):287–303

Sakuratani T (1981) A heat balance method for measuring water flux in the stem of intact plants. J Agri Meteorol 37(1):9–17

Sakuratani T (1984) Improvement of the probe for measuring water flow rate in intact plants with the stem heat balance method. J Agri Meteorol 40:273–277

Sellers PJ (1987) Canopy reflectance, photosynthesis, and transpiration, II. The role of biophysics in the linearity of their interdependence. Remote Sens Environ 21:143–183

Stannard DI (1993) Comparison of Penman-Monteith, Shuttleworth-Wallace, and Modified Priestley-Taylor Evapotranspiration Models for wildland vegetation in semiarid rangeland. Water Resour Res 29(5):1379–1392

Su Z (2000) Remote Sensing of land use and vegetation for mesoscale hydrological studies. Int J Remote Sens 21(2):213–233

Su Z (2002) The Surface Energy Balance System (SEBS) for estimation of turbulent heat fluxes. Hydrol Earth Syst Sci 6(1):85–99

Thomas J (1977) Leaf reflectance vs. leaf chlorophyll and carotenoid concentrations for eight crops. Agron J 69:799–810

Vertessy RA, Benyon RG, O'Sullivan SK (1995) Relationships between stem diameter, sapwood area, leaf area and transpiration in a young mountain ash forest [J]. Tree Physiol 15:559–608

Vertessy RA, Hatton TJ, Reece P, O'sullivan SK, Benyon GB (1997) Estimating stand water use of large mountain ash trees and validation of the sap flow measurement technique. Tree Physiol 17:747–756

Wang JH, Ma QL (2003) Study on restoration strategies, characteristics and status of degenerated artificial *Haloxylon ammodendron* communities at the edge of Minqin oasis. Acta Botanica Boreali-occidentalia Sinica 23(12):2107–2112

Whitley R, Medlyn B, Zeppel M (2009) Comparing the Penman–Monteith equation and a modified Jarvis-Stewart model with an artificial neural network to estimate stand-scale transpiration and canopy conductance. J Hydrol 373(1–2):256–266

Wullschleger SD, Meinzer FC, Vertessy RA (1998) A review of whole-plant water use studies in trees. Tree Physiol 18:499–512

Wullschleger SD, Hanson PJ, Todd DE (2001) Transpiration from a multi-species deciduous forest as estimated by xylem sap flow techniques. For Ecol Manage 143:205–213

Xie XQ (1991) The estimation of the daily evapotranspiration in cropland with the remote-sensing instantaneous surface temperature. Environ Remote Sens 6(4):253–260

Xu H (2006) Study on plants water consumption of Tarim desert highway protection forest. The PHD thesis of the graduate school of Chinese Academy of Sciences

Xu H, Li Y, Zou T, Xie JX, Jiang LX (2007) Ecophysiological response and morphological adjustment of *Haloxylon ammodendron* towards variation in summer precipitation. 27(12): 5019–5028

Xu H, Zhang XM, Yan HL (2008) The plant water status of the shelterbelt along the Tarim desert highway. Sci Bull 53:131–139

Zhai CX, Ma J, Li Y (2007) Soil evaporation of Aeolian sandy soil in Gurbantunggut desert. Arid Land Geogr 30(006):805–811

Zhang XY, Gong JD (2004) Study on volume and velocity of stem sap flow of *Haloxylon ammodendron* by heat-pulse technique. Acta Bot Boreal Occident Sin 24(1–2):2250–2254

Zhang XF, Micha P (2007) Preprocessing feature extraction and lithologic mapping using EO-1 Hyperion data. J Image Gr 12(6):981–990

Zhang XY, Gong JD, Zhou MX (2003) A study on the stem sap flow of *Populus euphrtaicr* and *Tamaris* spp. By heat pulse technique. J Glaciol Geocryol 25(5):584–590

Zhang JC, Zhao M, Zhang YC (2005) A research between photosynthetic, transpiration characteristic and impact of irrigated vegetation of *Haloxylon ammodendron* and *Nitraria tangutorum*. Acta Bot Boreal Occident Sin 25(1):0070–0076

Zhao YS (2003) The principles and methods of the analysis and applications of remote sensing. Science Press, Beijing

Zhao D, Reddy K, Kakani V (2005) Nitrogen deficiency effects on plant growth, leaf photosynthesis, and hyperspectral reflectance properties of sorghum. Eur J Agron 22:391–403